TECHNICAL TRANSACTIONS | CZASOPISMO TECHNICZNE
MECHANICS | MECHANIKA
2-M/2015

FILIP LISOWSKI*

NUMERICAL COMPUTATION OF STRESSES AND DEFORMATIONS IN THE PLANETARY ROLLER SCREW COMPONENTS

OBLICZENIA NUMERYCZNE NAPRĘŻEŃ I ODKSZTAŁCEŃ W ELEMENTACH PLANETARNEJ PRZEKŁADNI ŚRUBOWEJ ROLKOWEJ

Abstract

The paper presents finite element analysis of stresses and deformations of planetary roller screw components. The finite element model takes into account the frictional contact between helical surfaces. The results of numerical calculations for the contact problem were compared with the theoretical solution based on the Hertz theory. The obtained results can be used in the development of design procedures of planetary roller screw.

Keywords: *Planetary roller screw, finite element analysis, contact analysis*

Streszczenie

W artykule przedstawiono analizę naprężeń i odkształceń elementów planetarnej przekładni śrubowej rolkowej. W modelu MES uwzględniono kontakt z tarciem pomiędzy powierzchniami śrubowymi. Wyniki z obliczeń numerycznych dla zagadnienia kontaktowego porównano z rozwiązaniem teoretycznym w oparciu o wzory Hertza. Otrzymane wyniki mogą być wykorzystane w rozwoju procedur projektowych.

Słowa kluczowe: *Przekładnia śrubowa rolkowa, analiza MES, analiza kontaktu*

* M.Sc. Eng. Filip Lisowski, Institute of Machine Design, Faculty of Mechanical Engineering, Cracow University of Technology.

1. Introduction

Planetary Roller Screw (PRS) is a mechanical actuator that is characterized mainly by high efficiency, high load capacity, resistance to dynamic loads and resistance to a hostile work environment. In comparison with a more common ball screw, roller screws have larger contact surfaces of rolling elements, higher axial stiffness and lower noise. However, because of manufacturing (fine grinding, surface hardening) and unitary production PRS is much more expensive.

The main elements of a planetary roller screw (Fig. 1), which transfer the load, are: screw (1), nut (3) and rollers (2). The movement of the rollers is synchronized by the planetary toothed conjunction (4, 5). The cores of the rollers are based in the endplates (6).

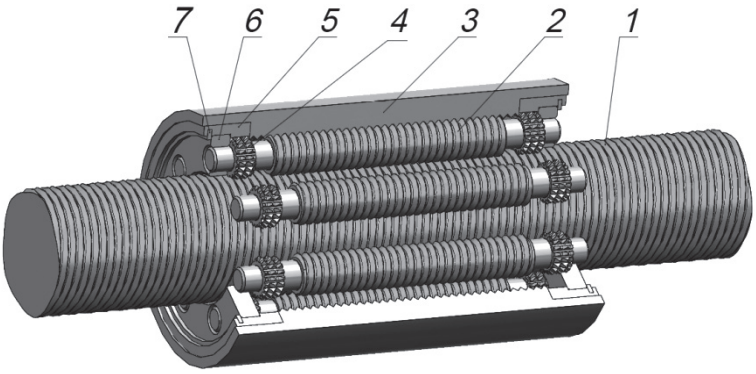

Fig. 1. Planetary roller screw structure; 1 – screw, 2 – roller, 3 – nut, 4 – satellite toothed wheel, 5 – end plate, 6 – sun toothed wheel, 7 – retaining wheel

The previous publication related to the stress analysis and the load distribution in the planetary roller screw components concerned mainly: the analysis of the displacements and the load distribution between cooperating elements and the related determination of the stiffness of the cooperating areas [2], analysis of the load distribution for the preliminary design based on the analytical model and a study on the load cases [5], the procedure of the preliminary design of PRS including also an analysis of the carrying capacity of the threads based on the Hertz theory [3], a mathematical model for contact analysis, where series of equivalent balls are used to replace the rounded profile of the roller's thread [8], an optimal design and contact analysis concerning an attempt to reduce the contact area between the screw, the roller and the nut for trapezoidal threads [4].

The main goal of this paper was to investigate displacements and stresses of the cooperating components of a planetary roller screw including the contact between the screw, the roller and the nut simultaneously. An additional objective was to investigate the shape of the contact regions on the thread's surfaces and to compare numerical results with the theoretical solution based on the Hertz theory.

The presented studies were carried out for the following pitch dimensions of the screw, roller and nut: d_s = 30 mm, d_r = 10 mm, d_n = 50 mm and the thread pitch p = 2 mm.

2. Theoretical solution of the contact problem

An approximate method of the solution to the problem of two bodies in contact, using the Hertz theory, was presented in [1, 7] and developed in [6]. The theory relates to the general case of compression of two elastic bodies with the radii of curvature for the first body: R_{11}, R_{12} and for the second body: R_{21}, R_{22} where $R_{11} < R_{12}$ and $R_{21} < R_{22}$. For the cooperation of the roller, screw and nut threads (Fig. 2), the radii of the curvatures were accepted as given in eq. 1–3, where indexes *r*, *s*, *n* refer consecutively to the roller, the screw and the nut.

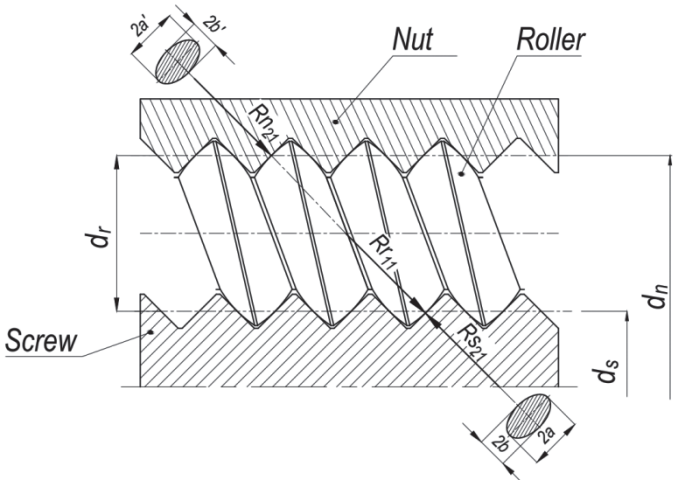

Fig. 2. Pitch diameters of planetary roller screw components and theoretical ellipse of contact

The following radii take into account respectively the curvatures of the threads' profiles and the curvatures of the helix lines.

$$Rr_{11} = \frac{d_r}{2\sin(\alpha_0)}, \qquad Rr_{12} = \frac{(d_r/2)^2 + p^2}{p} \tag{1}$$

$$Rs_{21} = \frac{(d_s/2)^2 + p^2}{p}, \qquad Rr_{12} = \infty \tag{2}$$

$$Rn_{21} = \frac{(d_n/2)^2 + p^2}{p}, \qquad Rr_{22} = \infty \tag{3}$$

where:

d_s, d_n, d_r – pitch diameter of the screw, the nut and the roller,
α_0 – thread flank angle,
p – thread pitch.

Contact pressures can be calculate using the eq. (4).

$$p_o = \frac{3}{2}\frac{F_c}{\pi \cdot a \cdot b} \tag{4}$$

where:

F_c – contact pressure force

a, b – semi-axes of the ellipse of contact determined from eq. (5).

$$a = m_H \sqrt[3]{\frac{3\pi F_c}{2}\frac{\kappa}{A+B}}, \quad b = n_H \sqrt[3]{\frac{3\pi F_c}{2}\frac{\kappa}{A+B}}, \quad \kappa = \frac{1-\nu^2}{\pi E} \tag{5}$$

where:

ν – Poisson's ratio,

E – Young's modulus.

Based on the coefficients A and B, depending on the radii of curvatures, an auxiliary angle θ is determined (eq. 6–7). For this angle, Hertz coefficients m_H and n_H appearing in eq. 5 can be determined.

$$\theta = \arccos\left(\frac{B-A}{A+B}\right), \quad A+B = \frac{1}{2}\left(\frac{1}{R_{11}}+\frac{1}{R_{12}}+\frac{1}{R_{21}}+\frac{1}{R_{22}}\right) \tag{6}$$

$$A-B = \frac{1}{2}\sqrt{\left(\frac{1}{R_{11}}-\frac{1}{R_{12}}\right)^2+\left(\frac{1}{R_{21}}-\frac{1}{R_{22}}\right)^2+2\left(\frac{1}{R_{11}}-\frac{1}{R_{12}}\right)\left(\frac{1}{R_{21}}-\frac{1}{R_{22}}\right)\cos(2\varphi)} \tag{7}$$

where:

φ – angle determining the relative position of contact planes.

The values of the Hertz coefficients can be taken from the tables in the literature [7] for $\theta \in \langle 30° \div 90° \rangle$ with an accuracy of 5° or in [1] $\theta \in \langle 1° \div 90° \rangle$ with an accuracy of 1°. Publication [6] also delivered continuous functions of Hertz coefficients m_H and n_H as given in eq. 8 and eq. 9.

$$m_H^{-1} = -0,72576 \cdot \theta^4 + 0,306757 \cdot \theta^3 - 0,425848 \cdot \theta^2 + 0,817353 \cdot \theta + 0,018040 \tag{8}$$

$$n_H = -0,640562 \cdot \theta^6 + 3,471455 \cdot \theta^5 - 7,405219 \cdot \theta^4 + 7,984778 \cdot \theta^3 - 4,592703 \cdot \theta^2 + \\ +1,771294 \cdot \theta + 0,108768 \tag{9}$$

3. Finite element analysis

The analysis of stresses and deformation was performed by applying ANSYS software. A finite element model (Fig. 3) included a 1/10 section of a planetary roller screw within a single cooperating pair of threads and was prepared using 20-node solid elements SOLID95 and contact elements TARGE170 and CONTA 174. Contact elements were defined on much larger areas than the surface areas resulting from the Hertz theory (Fig.4). Due to complex geometry of threads an irregular mesh was used. In the regions of contact, the mesh was refined with element size h = 0,01 mm. The coefficient of friction $\mu = 0.1$; Young modulus $E = 2{,}11 \cdot 10^5$ MPa and Poisson ratio $\nu = 0.3$ were accepted. The axial load, which was applied to the core of the nut, was accepted at the low, medium and high level $F = \{25, 50, 100\}$ N.

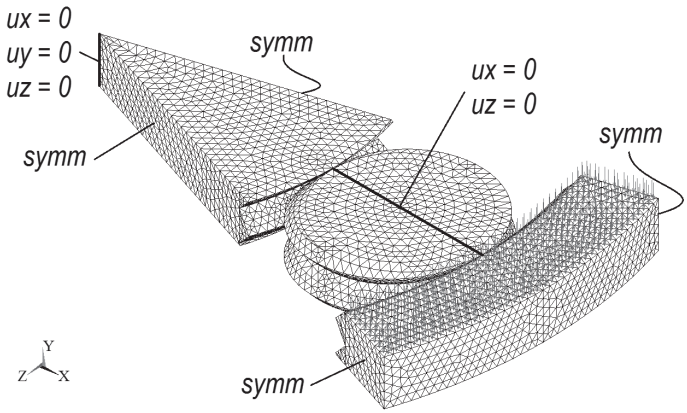

Fig. 3. Finite element model of 1/10 section of PRS with boundary conditions

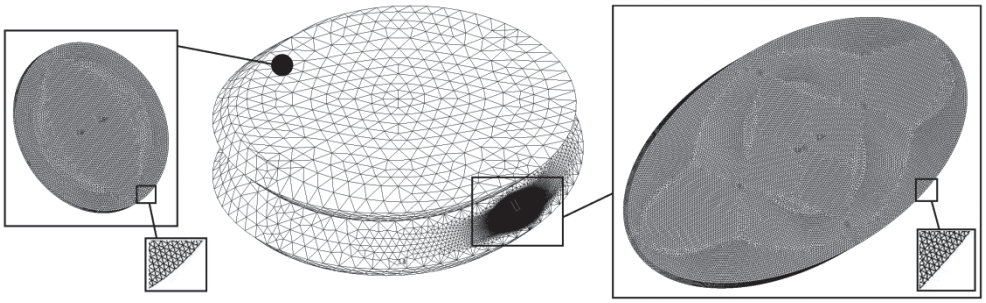

Fig. 4. Mesh refinement in the contact regions in example of the roller (element size h = 0.01 mm)

4. Results

The results obtained from the theoretical and finite element analysis are summarized in Tables 1–3. In Fig. 5 to Fig. 10 the results obtained for the axial load F = 50 N are presented.

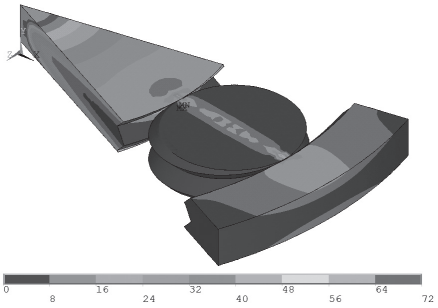

Fig. 5. Huber-Mises-Hencky reduced stress

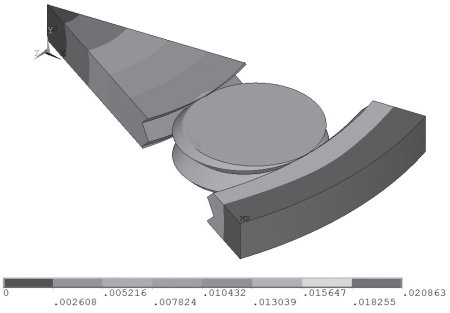

Fig. 6. Displacement vector sum

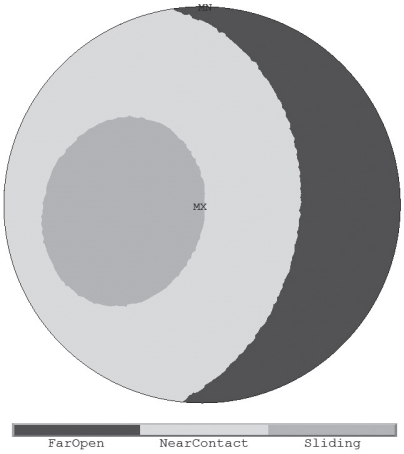

Fig. 7. Contact area between the roller and screw determined with FEA

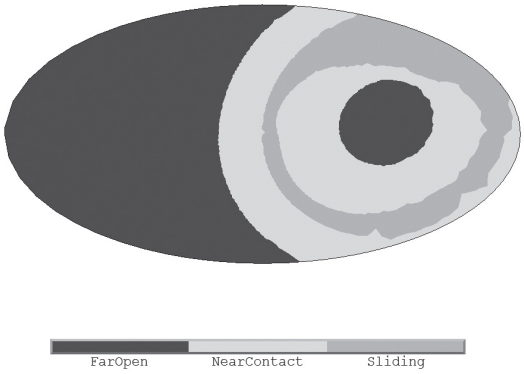

Fig. 8. Contact area between the roller and the nut determined with FEA (F = 50 N)

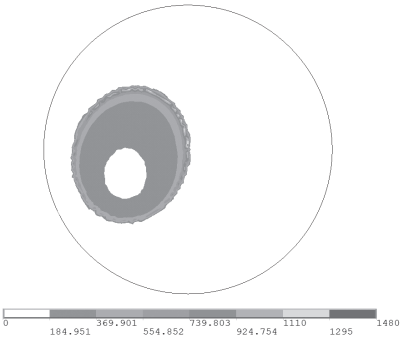

Fig. 9. Contact pressure between the roller and screw determined with FEA

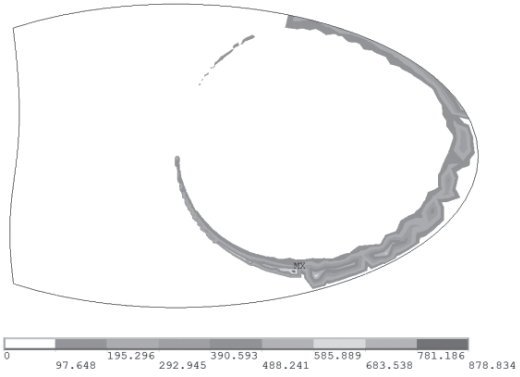

Fig. 10. Contact pressure between the roller and the nut determined with FEA

Fig. 5 and Fig. 6 present Huber-Mises-Hencky the sum of reduced stress and displacement vector. Fig. 7 and Fig. 8 show the contact areas determined based on FEM, with the indication of the sliding zone. The contact area between the screw and the roller is closed, but between the roller and the nut there is an edge zone. Fig. 9 and Fig. 10 present contact pressure between the screw roller and the nut. The difference in the contact pressure for numerical and theoretical solutions is at the level of 0–39% for the contact between the screw and roller and decreases with the increase of the axial load (Tab. 1). A similar result is obtained for the contact between the roller and the nut. For comparison, the pressure around the border of the sliding zone was taken. The difference of local displacements in the contact areas between the screw and roller as well as the roller and nut is about 16% (Tab. 3).

Table 1

Contact pressure and the contact regions between the roller and screw

Axial Load [N]	Contact pressure (Hertz) [MPa]	Contact pressure (FEM [MPa]	Relative error of contact pressure
25	999	608	39.1%
50	1259	1480	17.6%
100	1585	1586	0.1%

Table 2

Contact pressure and the contact regions between the roller and nut

Axial Load [N]	Contact pressure (Hertz) [MPa]	Contact pressure (FEM) [MPa]	Relative error of contact pressure
25	969	–	–
50	1221	879	28.0%
100	1585	1531	0.5%

Table 3

Axial displacement in the contact regions (FEM)

Axial Load	Axial displacement in contact region of screw (FEM)	Axial displacement in contact region of nut (FEM)	Displacement factor
F [N]	$u_{y\,(s-r)}$ [mm]	$u_{y\,(n-r)}$ [mm]	$u_{y\,(n-r)}/u_{y\,(s-r)}$
25	0.00654	–	–
50	0.01306	0.01519	1.16
100	0.02616	0.03064	1.17

5. Conclusions

The consistency of the theoretical and numerical results for the contact analysis was achieved only after a significant increase in the axial load. Using the finite element analysis gives good results at a medium and high level of the axial load. At low values of the axial load the results of the FEA should be assessed carefully.

In fact, the displacement can be larger due to the roughness of the surfaces, which in the FEM is omitted, and the displacements obtained from the FEM analysis for the low level of the axial load are comparable to roughness of the surfaces. For a high level of the axial load the influence of surface roughness on the accuracy of the cooperation can be omitted. It would be useful to carry out experimental studies verifying the influence of the surface roughness for a low load level.

References

[1] Cooper D.H., *Tables of Hertzian contact-stress coefficients*, University of Illinois, Report R-387, 1968.
[2] Lisowski F., *The Analysis of displacements and the load distribution between elements in a Planetary Roller Screw*, Applied Mechanics and Materials, Vol. 86, 2014, 361-364.
[3] Lisowski F., *Procedura wstępnego projektowania planetarnej przekładni śrubowej rolkowej z przekładnia zębatą*, Przegląd Mechaniczny, 4/2014, 39-49.
[4] Ma S., Liu G., Zhou J., Tong R., *Optimal design and contact analysis for Planetary Roller Screw*, Applied Mechanics and Materials, Vol. 86, 2012, 361-364.
[5] Ryś J., Lisowski F., *The computational model of the load distribution between elements in a planetary roller screw*, Journal of Theoretical and Applied Mechanics, Vol. 52, No. 3, 2014.
[6] Romanowicz P., Szybiński B., *Analytical and numerical assessment of fatigue properties in rolling bearings*, 4th International Conference on Integrity, Reliability & Failure, 2013.
[7] Timoshenko S., Goodier J.N., *Teoria sprężystości*, McGraw-Hill Book Company, 1951.
[8] Zhang X., Liu G., Ma S., Tong R., Luo H., *Study on axial contact deformation of planetary roller screw*, Applied Mechanics and Materials, Vol. 155–156, 2012, 779-783.